nanoenergy advances

MDPI

Communication

First-Principle Insights into Positive Triboelectrification of Polyoxymethylene Through Homolytic Bond Rupture

Giulio Fatti [1,*], Hyunseok Ko [2] and Sung Beom Cho [3]

[1] Tribology Group, Department of Mechanical Engineering, Imperial College London, London SW7 2BX, UK
[2] Division of Carbon Neutrality & Materials Digitalization, Korea Institute of Ceramic Engineering and Technology (KICET), Jinju 52851, Republic of Korea; hko@kicet.re.kr
[3] Department of Materials Science and Engineering, Ajou University, Suwon 16499, Republic of Korea; csb@ajou.ac.kr
* Correspondence: g.fatti18@imperial.ac.uk

Abstract: Understanding the mechanism underlying triboelectrification (TE) in polymers is crucial for developing cheap and effective triboelectric nanogenerators. Finding out how a polymer becomes tribopositive is especially relevant, as most polymers tend to charge negatively, reducing the power output and the range of applications. Thus far, it has remained unclear whether TE in polymers is to be attributed to homolytic ion transfer, heterolytic material transfer, or electronic transfer. Investigating the triboelectrification mechanism of polyoxymethylene by first-principle investigations, this study reveals a novel pathway driven by homolytic bond rupture. Our study demonstrates that the homolytic cleavage of a C–H bond upon contact with a metal surface drives a rearrangement in the oxidation state of the carbon atom, leading its dangling bond to cede an electron to the countersurface, leading to significant positive charging of the POM. This mechanism aligns with the triboelectric series and experimental observations. These insights suggest that TE mechanisms can be more complicated than heterolytic material transfer, depending on material-specific composition and chemistry. This study potentially paves the way for designing materials with tailored triboelectric properties for enhanced nanogenerator performance.

Keywords: triboelectrification; tribopositive materials; homolytic ion transfer; density functional theory; mechanochemistry

Academic Editor: Erik Kjeang

Received: 10 September 2024
Revised: 26 November 2024
Accepted: 10 January 2025
Published: 14 January 2025

Citation: Fatti, G.; Ko, H.; Cho, S.B. First-Principle Insights into Positive Triboelectrification of Polyoxymethylene Through Homolytic Bond Rupture. *Nanoenergy Adv.* **2025**, *5*, 1. https://doi.org/10.3390/nanoenergyadv5010001

1. Introduction

Since their invention a decade ago, triboelectric nanogenerators (TENGs) have attracted an increasing amount of attention from researchers. TENGs are energy-harvesting devices that can collect energy by converting mechanical energy into electricity. The collected energy can be stored in batteries [1,2] or directly used for self-powered electronics and sensors [3–5], as well as to provide stability to grid applications [6,7]. The overwhelming majority of TENGs use polymer-based triboelectric layers because of their low cost, flexibility, and larger charge output and stability [5,8,9]. However, a problem with polymer-based TENGs is that most polymers tend to behave as tribonegative materials [10–12]. According to the triboelectric series, materials can be ordered according to their ability to attract positive or negative charges [13]. This is done so that, when two materials are paired against each other, the material charging positively (negatively) is positioned higher (lower) in the series, iterating the process with many different materials to build a series. Because the maximum charge output depends on the distance between two materials in the

series, the fact that polymers mostly behave as tribonegative materials reduces the options to generate a large electric output, limiting TENGs' range of applicability.

This problem is hard to address, as the reason why polymers tend to be concentrated toward the negative spectrum of triboelectric materials is not entirely clear yet. In fact, researchers are still debating the mechanism through which polymers become triboelectrically charged [13]. This includes uncertainty about whether the charge carriers are electrons, ions, or fragments of material [14]. A series of experiments by Šutka and coworkers showed that triboelectric charging in polymer–polymer contact occurs via mechanochemically induced heterolytic bond cleavage and the transfer of charged microscopic fragments of materials across the contact interface [15,16]. This was consistent with the observation that triboelectric charging was higher for polymers with lower cohesive energy and higher mechanochemical activity [17,18]. In this picture, triboelectric charging is mainly driven by ions or fragments of material.

On the contrary, experiments conducted by Wang's group on polymer–metal contact showed that triboelectric charge carriers are mostly of electronic origin. By measuring thermionic and photoelectron emissions, they observed a charge dissipation profile coherent with the emission of electrons with a very low or inexistent presence of charged ions [19–21]. They observed that hotter (cooler) materials receive a positive (negative), consistent with the thermionic emission effect [22]. Another study on polytetrafluoroethylene (PTFE)–metal contact, corroborated by experimental results, showed that increasing triboelectric charging on PTFE is correlated with the homolytic bond cleavage of carbon–fluorine bonds. In this case, the transfer of neutral ions forms dangling bonds that are then saturated by electron transfer in the interaction with the metal surface [23]. Another study by Fu et al. corroborated this picture, showing that mechanoradicals were formed through homolytic bond cleavage in contact between PTFE and viscoelastic polymer adhesives composed by polyacrylates [24].

Here, we focused on polyoxymethylene (POM), a material positioned towards the positive end of the triboelectric series, and investigated its properties through first-principle density functional theory (DFT) calculations. We showed that homolytic bond cleavage can indeed contribute to triboelectric charging. Moreover, we uncover the chemical mechanism promoting the formation of positive tribocharges on POM, suggesting a strategy for the design of tribopositive materials.

2. Methods

The properties of POM over gold were investigated through plane-wave DFT as implemented in the VASP package [25,26]. The exchange–correlation potential was described by the Perdew–Burke–Ernzerhof (PBE) parametrization [27] of the generalized gradient approximation (GGA) with the Grimme correction (DFT-D2)s to take into account the van der Waals (vdW) interactions between polymer chains, and the ionic species were described using the projector-augmented plane wave (PAW) method [28]. The primitive cell of gold (Au) was downloaded from the Materials Project, while the crystal structure of polyoxymethylene (POM) was built using the experimental data provided in Ref. [29]. Both were further optimized with a variable cell relaxation. The lattice parameter converged at a cutoff of 400 eV, which was thus chosen to carry out calculations. The scaling parameter of the vdW correction was set at 0.42 to have comparable results with our previous studies [23,30]. The calculated lattice parameters were $a = 7.39$, $b = 7.75$, $c = 4.75$, in good agreement with the experimental values $a_{exp} = 7.12$, $b_{exp} = 7.65$, $c_{exp} = 4.77$. A slight overestimation of the lattice parameter is a well-known feature of the PBE functional. The relaxed cell is shown in Figure 1a. A $4 \times 4 \times 6$ Gamma-centered grid was employed to sample the Brillouin zone, and Gaussian broadening with a width of 0.05 eV was used to

calculate the partial occupancies. The convergence threshold for the minimization of the electronic structure was set to 10^{-6} eV, while the convergence threshold on the forces for structure relaxation was set to 10^{-2} eV/Å.

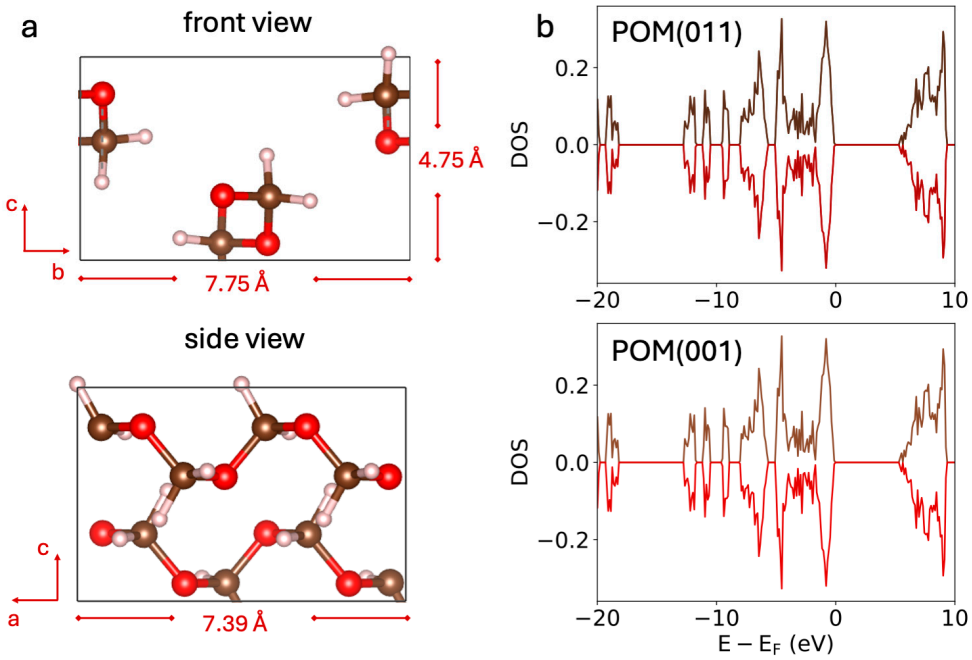

Figure 1. (**a**) Crystal structure of the POM relaxed unit cell with the lattice parameter values shown for each cell axis. The top panel shows a front view, highlighting the b and c axes, while the bottom panel shows a side view with the a and c axes highlighted. (**b**) Density of states of the POM(011) (top) and the POM(001) surface (bottom). The bottom panel also shows the DOS of POM(011), but it is not visible because of the complete overlap between the two DOSs.

The interfaces were prepared using the CoherentInterfaceBuilder tool as provided in the Pymatgen package [31]. The Builder imposes three constraints to generate the interfaces from bulk structures, the maximum strain on the lattice parameter and the angle, as well as the maximum surface area. We imposed a maximum 2% mismatch on the lattice parameters, a 2.5% mismatch on the angles, and a 250 ^{2} limit on the surface area, as the Builder could not find any match for smaller surface areas. To study the charge transfer at a POM–gold interface, we selected a 6-layer Au(111) slab, the most stable gold surface, in accordance with our previous studies [23,32]. For POM, we generated two different surface terminations, POM(001) and POM (011), to verify the effect of surface termination on the electronic structure and verify whether it affects the band gap and, thus, the charge transfer properties. The calculated density of states in Figure 1b shows that the two slab terminations have exactly the same electronic structure and are interchangeable. We did not test any other termination because, e.g., POM(111) would have required breaking the backbone O–C bond, which would have caused the fast degradation of the chain in the atmosphere [33]. Therefore, we selected a 3-layer POM(001) slab to match with Au(111). A 15 Å vacuum region was added above the interface to separate the periodic replicas along the z direction. This allowed us to have a 44 Å high slab, and a previous study found that 40 Å is enough to isolate the periodic replicas of interface charges [34]. We sampled the Brillouin zone only at the gamma point due to the large size of the cell. The partial charges were evaluated using Bader analysis [35–37]. The same methodology was employed to simulate contact between polyethylene and gold.

3. Results and Discussion

First, we simulated a pristine POM deposited on an Au(111) slab, whose configuration is shown in Figure 2a, to examine the occurrence of electronic charge transfer. We selected this pair because POM is widely considered one of the most tribopositive materials, while gold is usually placed towards the middle of the triboelectric series, making it a good "triboneutral" material for benchmarking. To do this, we positioned POM at a 2.5 Å vertical separation from the Au slab, with the distance calculated from the lowest hydrogen atoms. After relaxation, Bader analysis showed that no charge transfer occurred in either direction, which could have been expected because the POM electronic structure was stable. Every bond in the material was saturated; thus, POM could not acquire any additional electrons. This suggests that electronic transfer cannot, per se, be the main driver of triboelectric charging and that either heterolytic or homolytic bond cleavage and ion transfer are needed.

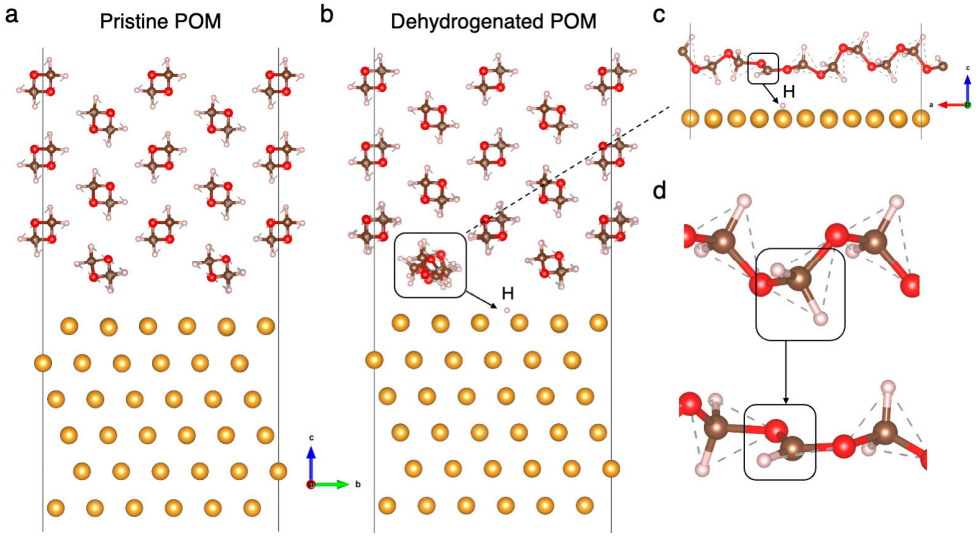

Figure 2. Structures of the simulated interface. Frontal view of (**a**) pristine and (**b**) dehydrogenated POM with the dehydrogenated chain highlighted; (**c**) side view of the dehydrogenated chain. The black box highlights the dehydrogenated carbon; (**d**) zoom-in on the structural deformation induced by C–H bond cleavage.

Therefore, we cleaved one C–H bond on the POM surface, transferred one hydrogen atom from POM to gold, and relaxed the structure again to investigate the effect of ion transfer on POM triboelectric charging. The relaxed configuration after hydrogen transfer is shown in Figure 2b,c, while the deformation induced by the hydrogen vacancy on the POM chain is highlighted in Figure 2d. The energy cost of cleaving the bond was calculated to be 1.2 eV. Although this energy is not achievable just by thermal fluctuations, it can be easily attained through mechanochemistry, as proven elsewhere [32]. The cleavage of the C–H bond is necessarily homolytic because DFT is a ground state method and cannot observe excited states, including the chemical separation of charged ions. Once the hydrogen atom is separated from carbon, DFT is not able to observe the transfer of electrons between the two atoms, and valence electrons flow back to their original ion. We consider this a realistic assumption, as the C–H bond is nonpolar.

Because the considered reaction CH + Au → C• + AuH is homolytic, a dangling bond is left on the carbon atom which can, in principle, behave either as an electron acceptor or donor. We performed Bader analysis again and found that POM carries a net positive charge of 0.55 e, indicating that the carbon acts as an electron donor. This is consistent with previous experimental findings that found POM on the positive side of the triboelectric series. This is shown in Figure 3, which compares a triboelectric series built from reports in

the literature (arrow on top) with the calculated charging obtained from DFT here and in previous work [32] (bars on the bottom part). This shows that POM triboelectric charging is indeed very high, being of the same order of magnitude as materials towards the very end of the triboelectric series. For instance, silica is one of the most tribonegative materials and was observed to gain a negative charge −0.7 e, similar in magnitude to the 0.55 e observed here. These results, consistent with previous experimental and computational reports, suggest that homolytic bond cleavage successfully captures the charging mechanism of POM.

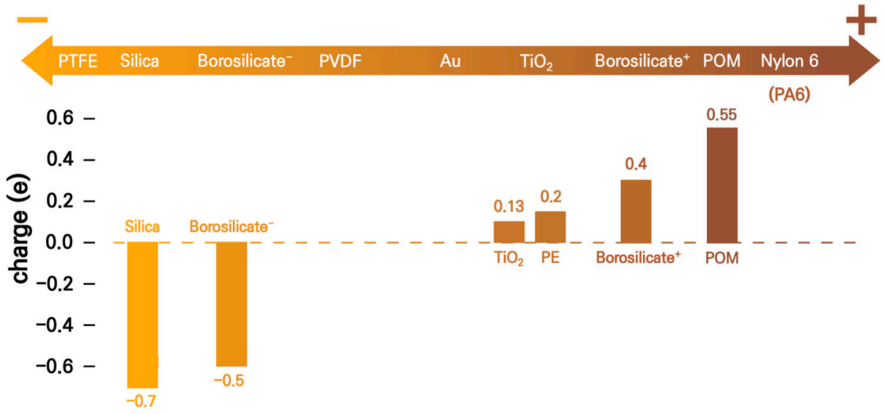

Figure 3. A semiquantitative triboelectric series built with data from different experimental sources (top arrow) [10,12] is compared with a series built with computational data from our calculations here and in our previous work about triboelectrification in silica–composite materials [32] (bottom bars).

This also provides insights into the mechanism generating tribopositive materials. Before C–H bond cleavage, every carbon is bonded to two oxygens and two hydrogens, resulting in the oxidation numbers shown in Figure 4a. However, the C–O bond is polar, while C–H is not, meaning that the actual charges on the atoms do not exactly correspond to the oxidation numbers. As described in Figure 4b, Bader analysis shows that oxygens have a calculated valence charge of 7.5 e, corresponding to a −1.5 e charge with respect to oxygen's neutral state. On the other hand, the oxidation number of hydrogens is 1+, but their calculated valence charge is 0.9 e, meaning they donate a charge of only 0.1 e to carbon. As a consequence, carbon shows a calculated valence charge of 2.5 e, i.e., a positive 1.5 e charge, despite its formal oxidation state being neutral.

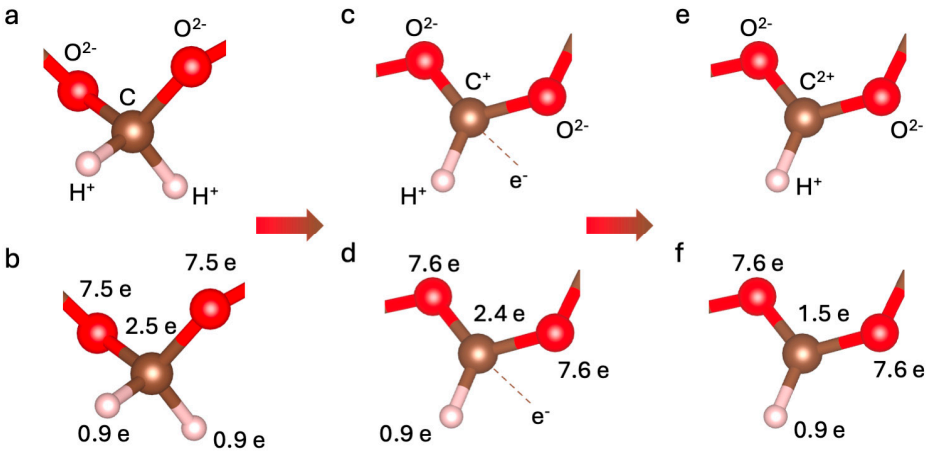

Figure 4. (**a**) Formal oxidation numbers of atoms and (**b**) calculated valence charges in a pristine POM monomer; (**c**) change in oxidation state and (**d**) actual calculated charge after cleavage of one C–H bond and the introduction of a dangling bond; (**e**) final oxidation state and (**f**) actual calculated charge after C donates one electron to gold.

After hydrogen transfer, the formal oxidation number of carbon changes. Because it still donates electronic charge to the oxygens but does not accept it from the detached hydrogen anymore, its oxidation state switches from neutral to C^+. As shown in Figure 4c, oxygens and the remaining hydrogen keep their respective oxidation states (O^{2-} and H^+). However, we observed a slightly higher electronic charge on the oxygens, increasing from 7.5 e to 7.6 e (Figure 4d). This indicates that the carbon with a dangling bond loses further electronic charge to the oxygens and becomes more positively charged. This increased positivity and the instability of the dangling bond promote further transfer of charge towards Au, with the final calculated carbon charge equal to 1.5 e, corresponding to a C^{2+} oxidation state (Figure 4e,f).

The key element in this is the presence of oxygens in the backbone. Their high electronegativity attracts electronic charge from the dangling-bond carbon atom, making it donate its excess charge to the countersurface and favoring POM tribopositivity. To confirm this, we performed an analogous calculation with polyethylene (PE), which has a carbon-only backbone, with the formula $(–CH_2–)_n$. In PE, when a similar dangling bond was introduced by cleaving a C–H bond, the calculated charge was only 0.2 e, showing a different chemical mechanism. Interestingly, previous experimental reports showed that hetero-catenary polymers, i.e., polymers with elements other than carbon atoms in the backbone, are mostly positioned towards the positive end of the triboelectric series [11]. This indicates that introducing highly electronegative elements in the backbone can promote tribopositive behavior, suggesting a design principle for tribopositive materials.

4. Conclusions

In this work, we showed that homolytic ion transfer can be a major contribution to the triboelectric charging of polymers. Studying the contact between POM and gold, we found that transferring one hydrogen from POM to gold promotes the formation of a large positive charge, in agreement with previous reports, according to which, POM is a strong tribopositive material. The analysis of the calculated charges showed that the key to the formation of a positive charge is the presence of highly electronegative oxygens in the backbone chain of POM. Once a C–H bond is broken, the backbone carbon is left with an unstable dangling bond which can, in principle, act either as an electron donor or acceptor. However, the dangling-bond carbon is bonded to electronegative elements that attract additional electronic charge, making the carbon positive. This makes it favorable for the carbon atom to donate its remaining electronic charge to the gold countersurface, making POM highly positive. This suggests that introducing electronegative elements in a polymer backbone is a pathway to design tribopositive polymers.

Author Contributions: Conceptualization, G.F. and S.B.C.; methodology, G.F.; validation, H.K. and S.B.C.; resources, H.K.; data curation, G.F.; writing—original draft, G.F.; writing—review and editing, H.K. and S.B.C.; visualization, G.F.; supervision, H.K. and S.B.C.; project administration, H.K. and S.B.C.; funding acquisition, H.K. and S.B.C. All authors have read and agreed to the published version of the manuscript.

Funding: P This research was supported by the National R&D Program through the National Research Foundation of Korea (NRF) funded by the Ministry of Science and ICT (RS-2023-00209910 and RS-2023-00285390). G.F. acknowledges support from the ESPRC grant EP/X026582/1.

Data Availability Statement: The original contributions presented in the study are included in the article, further inquiries can be directed to the corresponding author.

Conflicts of Interest: The authors declare no conflict of interest.

References

1. Zhang, B.; He, L.; Zhang, R.; Yuan, W.; Wang, J.; Hu, Y.; Zhao, Z.; Zhou, L.; Wang, J.; Wang, Z.L. Achieving Material and Energy Dual Circulations of Spent Lithium-Ion Batteries via Triboelectric Nanogenerator. *Adv. Energy Mater.* **2023**, *13*, 2301353. [CrossRef]
2. Dong, K.; Wang, Z.L. Self-charging power textiles integrating energy harvesting triboelectric nanogenerators with energy storage batteries/supercapacitors. *J. Semicond.* **2021**, *42*, 101601. [CrossRef]
3. Kwak, S.S.; Yoon, H.-J.; Kim, S.-W. Textile-Based Triboelectric Nanogenerators for Self-Powered Wearable Electronics. *Adv. Funct. Mater.* **2019**, *29*, 1804533. [CrossRef]
4. Huang, T.; Zhang, Y.; He, P.; Wang, G.; Xia, X.; Ding, G.; Tao, T.H. "Self-Matched" Tribo/Piezoelectric Nanogenerators Using Vapor-Induced Phase-Separated Poly(vinylidene fluoride) and Recombinant Spider Silk. *Adv. Mater.* **2020**, *32*, 1907336. [CrossRef]
5. Wang, Z.L. Triboelectric Nanogenerators as New Energy Technology for Self-Powered Systems and as Active Mechanical and Chemical Sensors. *ACS Nano* **2013**, *7*, 9533–9557. [CrossRef]
6. Zhang, C.; Liu, Y.; Zhang, B.; Yang, O.; Yuan, W.; He, L.; Wei, X.; Wang, J.; Wang, Z.L. Harvesting Wind Energy by a Triboelectric Nanogenerator for an Intelligent High-Speed Train System. *ACS Energy Lett.* **2021**, *6*, 1490–1499. [CrossRef]
7. Cao, X.; Xiong, Y.; Sun, J.; Xie, X.; Sun, Q.; Wang, Z.L. Multidiscipline Applications of Triboelectric Nanogenerators for the Intelligent Era of Internet of Things. *Nano-Micro Lett.* **2022**, *15*, 14. [CrossRef]
8. Yang, P.; Shi, Y.; Tao, X.; Liu, Z.; Dong, X.; Wang, Z.L.; Chen, X. Radical anion transfer during contact electrification and its compensation for charge loss in triboelectric nanogenerator. *Matter* **2023**, *6*, 1295–1311. [CrossRef]
9. Zhao, L.; Zheng, Q.; Ouyang, H.; Li, H.; Yan, L.; Shi, B.; Li, Z. A size-unlimited surface microstructure modification method for achieving high performance triboelectric nanogenerator. *Nano Energy* **2016**, *28*, 172–178. [CrossRef]
10. Gooding, D.M.; Kaufman, G.K. Tribocharging and the Triboelectric Series. In *Encyclopedia of Inorganic and Bioinorganic Chemistry*; John Wiley & Sons, Ltd.: Hoboken, NJ, USA, 2019; pp. 1–14. ISBN 978-1-119-95143-8.
11. Chen, Q.; Shang, H.; Cheng, B.; Lu, C.; Wang, Y.; Zhang, Y.; Shao, T. Quantifying triboelectric series of polymers based on the measurement of triboelectrification with NaCl solution. *Chem. Eng. J.* **2024**, *488*, 150871. [CrossRef]
12. Diaz, A.F.; Felix-Navarro, R.M. A semi-quantitative tribo-electric series for polymeric materials: The influence of chemical structure and properties. *J. Electrost.* **2004**, *62*, 277–290. [CrossRef]
13. Lacks, D.J.; Shinbrot, T. Long-standing and unresolved issues in triboelectric charging. *Nat. Rev. Chem.* **2019**, *3*, 465–476. [CrossRef]
14. Li, J.; Shepelin, N.A.; Sherrell, P.C.; Ellis, A.V. Poly(dimethylsiloxane) for Triboelectricity: From Mechanisms to Practical Strategies. *Chem. Mater.* **2021**, *33*, 4304–4327. [CrossRef]
15. Lapčinskis, L.; Linarts, A.; Mālnieks, K.; Kim, H.; Rubenis, K.; Pudzs, K.; Smits, K.; Kovaļovs, A.; Kalniņš, K.; Tamm, A.; et al. Triboelectrification of nanocomposites using identical polymer matrixes with different concentrations of nanoparticle fillers. *J. Mater. Chem. A* **2021**, *9*, 8984–8990. [CrossRef]
16. Šutka, A.; Mālnieks, K.; Lapčinskis, L.; Kaufelde, P.; Linarts, A.; Bērziņa, A.; Zābels, R.; Jurķāns, V.; Gorņevs, I.; Blūms, J.; et al. The role of intermolecular forces in contact electrification on polymer surfaces and triboelectric nanogenerators. *Energy Environ. Sci.* **2019**, *12*, 2417–2421. [CrossRef]
17. Šutka, A.; Linarts, A.; Mālnieks, K.; Stiprais, K.; Lapčinskis, L. Dramatic increase in polymer triboelectrification by transition from a glassy to rubbery state. *Mater. Horiz.* **2020**, *7*, 520–523. [CrossRef]
18. Lapčinskis, L.; Mālnieks, K.; Blūms, J.; Knite, M.; Oras, S.; Käämbre, T.; Vlassov, S.; Antsov, M.; Timusk, M.; Šutka, A. The Adhesion-Enhanced Contact Electrification and Efficiency of Triboelectric Nanogenerators. *Macromol. Mater. Eng.* **2020**, *305*, 1900638. [CrossRef]
19. Li, S.; Zhou, Y.; Zi, Y.; Zhang, G.; Wang, Z.L. Excluding Contact Electrification in Surface Potential Measurement Using Kelvin Probe Force Microscopy. *ACS Nano* **2016**, *10*, 2528–2535. [CrossRef]
20. Xu, C.; Zhang, B.; Wang, A.C.; Cai, W.; Zi, Y.; Feng, P.; Wang, Z.L. Effects of Metal Work Function and Contact Potential Difference on Electron Thermionic Emission in Contact Electrification. *Adv. Funct. Mater.* **2019**, *29*, 1903142. [CrossRef]
21. Lin, S.; Xu, L.; Zhu, L.; Chen, X.; Wang, Z.L. Electron Transfer in Nanoscale Contact Electrification: Photon Excitation Effect. *Adv. Mater.* **2019**, *31*, 1901418. [CrossRef]
22. Lin, S.; Xu, L.; Xu, C.; Chen, X.; Wang, A.C.; Zhang, B.; Lin, P.; Yang, Y.; Zhao, H.; Wang, Z.L. Electron Transfer in Nanoscale Contact Electrification: Effect of Temperature in the Metal–Dielectric Case. *Adv. Mater.* **2019**, *31*, 1808197. [CrossRef] [PubMed]
23. Fatti, G.; Ciniero, A.; Ko, H.; Lee, H.U.; Na, Y.; Jeong, C.K.; Lee, S.-G.; Kwak, D.; Park, K.-I.; Cho, S.B.; et al. Rational Design Strategy for Triboelectric Nanogenerators Based on Electron Back Flow and Ionic Defects: The Case of Polytetrafluoroethylene. *Adv. Electron. Mater.* **2023**, *9*, 2300333. [CrossRef]
24. Fu, H.; Gong, J.; Cao, J.; Zhang, Z.; Long, Z.; Yang, B.; Chen, J.; Chen, Y.; Tao, X. Understanding contact electrification via direct covalent bond cleavage of polymer chains for ultrahigh electrostatic charge density. *Energy Environ. Sci.* **2024**, *17*, 3776–3787. [CrossRef]
25. Kresse, G.; Furthmüller, J. Efficiency of ab-initio total energy calculations for metals and semiconductors using a plane-wave basis set. *Comput. Mater. Sci.* **1996**, *6*, 15–50. [CrossRef]

26. Kresse, G.; Furthmüller, J. Efficient iterative schemes for ab initio total-energy calculations using a plane-wave basis set. *Phys. Rev. B* **1996**, *54*, 11169–11186. [CrossRef]
27. Perdew, J.P.; Burke, K.; Ernzerhof, M. Generalized Gradient Approximation Made Simple. *Phys. Rev. Lett.* **1996**, *77*, 3865–3868. [CrossRef]
28. Kresse, G.; Joubert, D. From ultrasoft pseudopotentials to the projector augmented-wave method. *Phys. Rev. B* **1999**, *59*, 1758–1775. [CrossRef]
29. Carazzolo, G.; Mammi, M. Crystal structure of a new form of polyoxymethylene. *J. Polym. Sci. A* **1963**, *1*, 965–983. [CrossRef]
30. Fatti, G.; Righi, M.C.; Dini, D.; Ciniero, A. Ab Initio Study of Polytetrafluoroethylene Defluorination for Tribocharging Applications. *ACS Appl. Polym. Mater.* **2020**, *2*, 5129–5134. [CrossRef]
31. Ong, S.P.; Richards, W.D.; Jain, A.; Hautier, G.; Kocher, M.; Cholia, S.; Gunter, D.; Chevrier, V.L.; Persson, K.A.; Ceder, G. Python Materials Genomics (pymatgen): A robust, open-source python library for materials analysis. *Comput. Mater. Sci.* **2013**, *68*, 314–319. [CrossRef]
32. Fatti, G.; Kim, H.; Sohn, C.; Park, M.; Lim, Y.; Li, Z.; Park, K.-I.; Szlufarska, I.; Ko, H.; Jeong, C.K.; et al. Uncertainty and Irreproducibility of Triboelectricity Based on Interface Mechanochemistry. *Phys. Rev. Lett.* **2023**, *131*, 166201. [CrossRef] [PubMed]
33. Archodoulaki, V.-M.; Lüftl, S.; Koch, T.; Seidler, S. Property changes in polyoxymethylene (POM) resulting from processing, ageing and recycling. *Polym. Degrad. Stab.* **2007**, *92*, 2181–2189. [CrossRef]
34. Fatti, G.; Restuccia, P.; Calandra, C.; Righi, M.C. Phosphorus Adsorption on Fe(110): An ab Initio Comparative Study of Iron Passivation by Different Adsorbates. *J. Phys. Chem. C* **2018**, *122*, 28105–28112. [CrossRef]
35. Henkelman, G.; Arnaldsson, A.; Jónsson, H. A fast and robust algorithm for Bader decomposition of charge density. *Comput. Mater. Sci.* **2006**, *36*, 354–360. [CrossRef]
36. Sanville, E.; Kenny, S.D.; Smith, R.; Henkelman, G. Improved grid-based algorithm for Bader charge allocation. *J. Comput. Chem.* **2007**, *28*, 899–908. [CrossRef]
37. Tang, W.; Sanville, E.; Henkelman, G. A grid-based Bader analysis algorithm without lattice bias. *J. Phys. Condens. Matter* **2009**, *21*, 84204. [CrossRef]